JOURNAL OF MATERIALS SCIENCE 22 (1987) 4439–4445

Electrical property and defect structure of lanthanum-doped polycrystalline barium titanate

S. SHIRASAKI, H. HANEDA
National Institute for Research in Inorganic Materials, Namiki 1-1, Sakura-Mura, Niihari-Gun, Ibaraki, Japan

K. ARAI, M. FUJIMOTO
Taiyō Yūden Co., Haruna-Chō, Gunma-Gun, Gunma, Japan

Electrical conductivity of two types of lanthanum-doped barium titanate ceramics with different dopant levels was measured at temperatures between 900 and 1250° C and P_{O_2} from 10^{-5} to 1 atm. The activation energies of the conduction for the two are interpreted in terms of the formation energy of ionized oxygen vacancies even in such a high P_{O_2} region. This fact is in contrast with a well-known controlled-valency model proposed for rare-earth-doped semiconducting perovskites. In a lightly lanthanum-doped specimen, semiconduction achieved at elevated temperatures is retained on cooling the specimen to room temperature, whereas in a heavily doped specimen, the resultant high-temperature semiconduction changed to insulation on cooling. The former behaviour on cooling is successfully explained by a metastabilization of oxygen vacancies accompanied by electrons formed at elevated temperatures.

1. Introduction

It is well known that n-type semiconduction can easily be achieved by doping lanthanum into barium titanate and then firing at temperatures above about 1300° C. Saburi has previously proposed a hopping model in a possible composition $Ba^{2+}_{1-x}La^{3+}_{x}Ti^{3+}_{x}Ti^{4+}_{1-x}O_3$ for a limited amount of lanthanum doping [1]. Many other researchers believed that carriers in the doped material essentially originate from donors yielded from La^{3+} replacing Ba^{2+} [2, 3]. Many difficulties have been encountered in these two controlled valency models. The former model is not in harmony with the fact that no Ti^{3+} ESR signal was detected in the doped semiconducting material [4], as well as in a hydrogen-reduced undoped barium titanate even at liquid nitrogen temperature [5]. Moreover, if these two models are the case, one cannot explain the experimental fact that Ag^{+} doping into barium titanate also resulted in n-type semiconduction [6]. A decisive difficulty is that both models indicate that semiconduction is exhibited just when lanthanum dissolves into barium sites in barium titanate. This was not the case; although lanthanum dissolved completely on firing the doped specimen at $\approx$ 1000° C, as far as could be detected by X-ray diffraction, the resultant material exhibited insulation [7].

In an effort to remove these difficulties, we have proposed a new semiconducting mechanism at high temperatures of doped barium titanate [8, 9]. This can be summarized as follows: the extra plus charge carried due to replacing Ba^{2+} by La^{3+} is essentially compensated by the formation of cation vacancies in barium and/or titanum sites. The occurrence of barium site vacancies may weaken the bond strength of the oxygen sublattice with respect to cations. As a result, when the doped material is fired at elevated temperatures, thermal dissociation of the oxygen sublattice readily occurs, by which oxygen vacancies with electrons or ionized oxygen vacancies form. The resultant electrons cause n-type semiconduction. One of the purposes of the present study is to acquire a greater understanding of the semiconducting behaviour of lanthanum-doped materials at elevated temperatures.

A lightly lanthanum-doped semiconductor has been used widely as a thermistor with a positive temperature coefficient of resistivity (PTCR), and as the host of a barrier layer-type of capacitor. It is important that the doped semiconductor is generally useful around room temperature. Therefore, a knowledge of both structural and conductivity changes in the semiconducting material formed at elevated temperatures on cooling to room temperature, is also necessary for a thorough understanding of the conduction behaviour of doped materials.

In the research and development of functional ceramics in general, however, it is important to note the reproducibility and reliability of the function, as well as the grade of it. We can generally say that lack of reproducibility and reliability is closely related to the occurrence of structures with nonequilibrium character. A knowledge of such metastable structures formed during the course of ceramic preparation is therefore important. Emphasis in this study is placed on the formation of metastable oxygen vacancies during cooling of the doped semiconductor formed at

0022–2461/87 $03.00 + .12

high temperatures. For those purposes, electrical conductivity as functions of P_{O_2} and temperature, and oxygen self-diffusion coefficient as a function of temperature of the doped ceramics, were measured and discussed.

2. Experimental methods

2.1. Preparation of specimens

Powders of guaranteed reagents of $BaCO_3$ (Wako Junyaku Co.) and TiO_2 (Kishida Kagaku Co.) and 99.9% pure La_2O_3 (Rare Metals Co.) were used as starting materials. They were intimately mixed wet for 20 h with a ball mill and ethanol as the medium with compositions of $x = 0.001$ and 0.01 in $Ba_{1-x}La_xTiO_{3+\delta}$, and then calcined at 1100° C for 2 h in air. The resultant powdered materials were pressed hydrostatically at about 1 ton cm^{-2} and then sintered at 1400° C for 4 h in air. The two types of sintered specimens I ($x = 0.001$) and II ($x = 0.01$) were cooled slowly (cooling rate = 180° C h^{-1}) or quenched to room temperature.

The sintered and then slowly cooled specimens were also crushed, and the resulting particles were screened by sieves to collect 14 to 16 (1.19 to 1.00 mm opening), 32 to 48 (0.50 to 0.297 mm), 60 to 100 (0.25 to 0.149 mm) and 200 to 325 (0.074 to 0.044 mm) mesh particles. To remove ultrafine particles attached to the surfaces of these mesh particles during crushing, they were washed in ethanol with the aid of an ultrasonic generator. The two resultant types of specimens with different particle sizes were used for oxygen diffusion measurements. The average grain sizes of these polycrystalline particles was determined by SEM and found to be 25.6 μm (specimen I) and 0.48 μm (specimen II), respectively.

2.2. Measurement of electrical conductivity

The electrical conductivity specimens were cut from the sintered tablets to rectangular slabs of approximate size 0.6 mm × 9 mm × 20 mm. The electrical contacts for the four-probe conductivity specimens were made by wrapping the specimens with thin platinum wires. The electrical conductivity was measured at room temperature and also as a function of P_{O_2} in the temperature range 900 to 1250° C. The oxygen partial pressure was regulated between 1 and 10^{-5} atm using $Ar-O_2$ mixtures. The details of the experimental apparatus and procedure have often been described elsewhere [4].

2.3. Measurement of oxygen diffusion coefficients

The self-diffusion coefficients of oxygen were determined by measuring the exchange rate of oxygen between an oxygen gas phase and the heated polycrystalline mesh particles over the temperature range 917 to 1375° C. Oxygen gas enriched with about 20% ^{18}O was used as the tracer. The reaction chamber used for the exchange was made of transparent silica glass whose outer surfaces were cooled by circulating water to minimize the exchange between the constituent oxygen of the chamber and the enriched oxygen gas. All diffusion anneals were undertaken with about $P_{O_2} = 50$ mm Hg. The amount of ^{18}O in the gas phase was traced as a function of diffusion annealing time using a mass-spectrometer.

The Crank relation was used to calculate D [10],

$$\frac{M_t}{M_\infty} = 1 - \sum_{n=1}^{\infty} \frac{6\alpha(\alpha + 1)\exp(-Dq_n^2 t/a^2)}{9 + 9\alpha + q_n^2\alpha^2} \quad (1)$$

where q is the nonzero roots of $\tan q_n = 3q_n/(3 + \alpha q_n^2)$, a is the solid sphere radius, α is the gram atom ratio of oxygen present in the solid particles to that in the gas phase, and M_t/M_∞ is the total amount of solute in the sphere after time t as a function of the corresponding quantity after infinite time.

TABLE I Resistivity of specimens I and II at room temperature

Specimen	Resistivity (Ω^{-1} cm^{-1})	
	Quenched	Cooled slowly
Specimen I	Several tens	Several tens
Specimen II	≈ 100	≈ 10^9

3. Results

3.1. Electrical conductivity at room temperature

Two types of specimen with $x = 0.001$ (specimen I) and $x = 0.01$ (specimen II) sintered at 1400° C for 4 h were slowly cooled and quenched to room temperature, respectively. The resistivities at room temperature of the four resultant specimens whose relative densities were above 96.0%, are shown in Table I. As seen there, both quenched specimens exhibit semiconduction whereas on slowly cooling them, specimen I remains semiconductive but specimen II changes to an insulator. It is quite important to clarify the origin of such a difference for a thorough understanding of the conductivity behaviour of lanthanum-doped materials.

3.2. Electrical conductivity as a function of P_{O_2} at elevated temperatures

Fig. 1 shows the P_{O_2} dependence of electrical conduc-

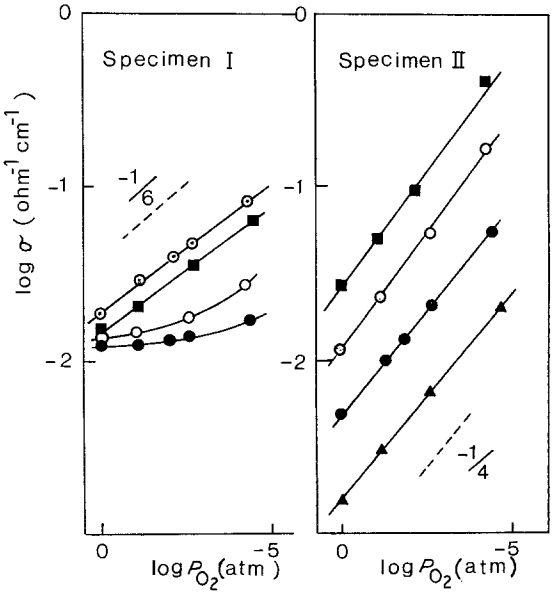

Figure 1 Electrical conductivity of specimens I and II ceramics at high temperatures as a function of P_{O_2}. (⊙) 1250° C, (■) 1200° C, (○) 1100° C, (●) 1000° C, (▲) 900° C.

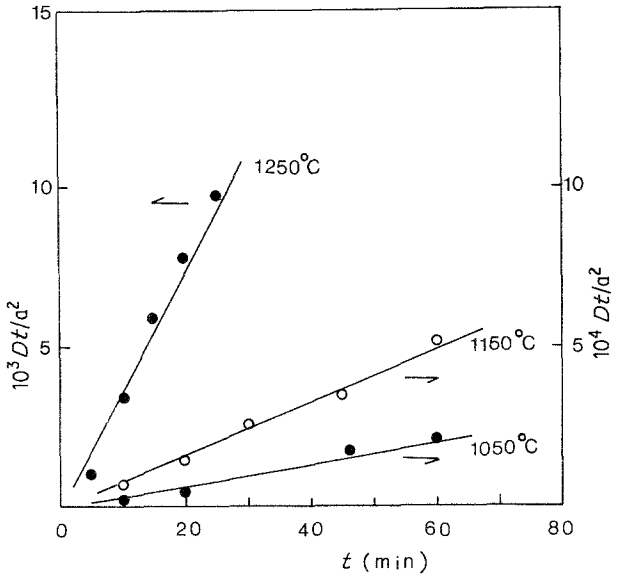

Figure 2 Typical plots of Dt/a^2 against time for particles of specimens I (○) and II (●).

tivity, σ, at elevated temperatures for specimens I and II which were cooled slowly after sintering. The average slope of the log–log plots for specimen II was found to be $-1/4.1$. In this specimen the two data points of σ at a P_{O_2} measured after measurements at a higher P_{O_2} and at a lower P_{O_2}, respectively, agreed well, indicating the σ to be attained at a complete equilibrium between temperature and P_{O_2}.

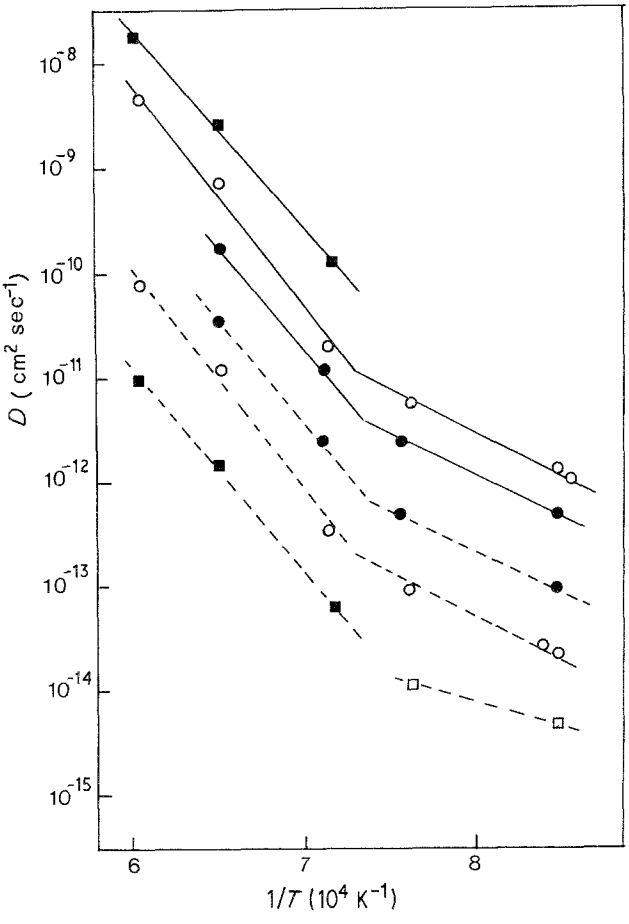

Figure 3 Temperature dependence of D_a of oxygen for polycrystalline particles of specimens I with different sizes. The calculations of D_a were made as (——) $a = a_p$ and (– – –) $a = a_g$, respectively. (□) 14 to 16, (■) 32 to 48, (○) 60 to 100, (●) 200 to 325 mesh.

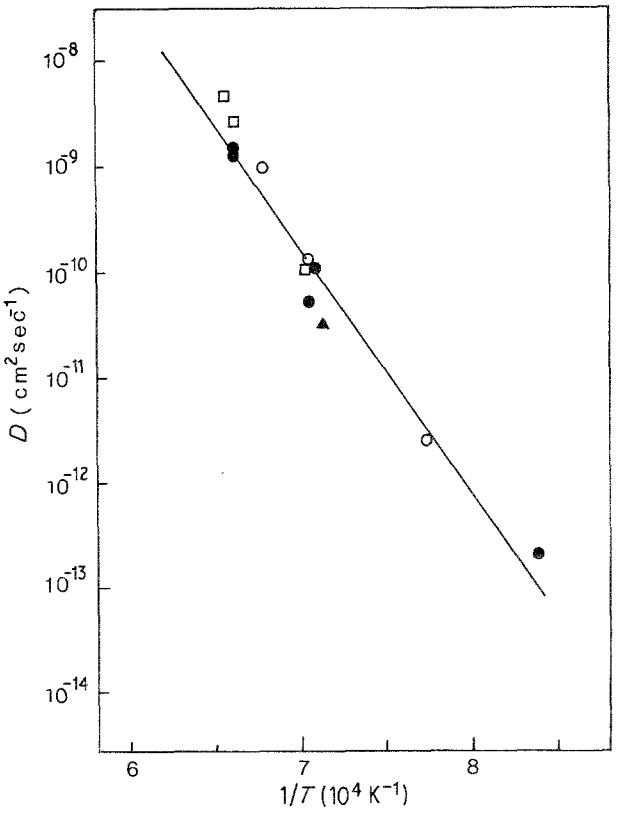

Figure 4 An Arrhenius plot of volume diffusion coefficient of oxygen for polycrystalline particles of specimen II. The calculations of D were made as $a = a_p$. (■) 14 to 16, (▲) 32 to 48, (○) 60 to 100, (●) 200 to 325 mesh.

In specimen I, on the other hand, the P_{O_2} dependence of σ shows a peculiar behaviour. It is noted that the log–log plots do not show straight lines in the runs at 1000 and 1100° C. The straight line plots result in the runs at 1200 and 1250° C, and their average slope was $-1/6.9$. It should be noted that the constancy of σ with time in all runs studied, was attained within 10 h in specimen II whereas a prolonged time of more than 40 h was necessary for achieving a rough constancy of σ with time in specimen I.

3.3. Volume diffusion coefficients of oxygen

Oxygen volume diffusion coefficients of polycrystalline specimens I and II were measured in an effort to obtain some knowledge of their oxygen vacancy levels. Fig. 2 shows typical plots of time, t, against the dimensionless quantity, Dt/a^2 determined by using Equation 1. The plots show straight lines passing through the origin. This suggests that the surface exchange reaction is not important. One can tentatively calculate apparent diffusivities, D_a, by using either the grain radius, a_g, or the particle radius, a_p, for the value of a in Equation 1. Fig. 3 illustrates Arrhenius plots of D_a for specimen I with different particle sizes; D_a was calculated in two ways by taking both the grain radius ($= 12.8\,\mu m$) and particle radius for the a value. As seen there, the diffusion data vary considerably with particle size as well as the choice of a = grain radius or a = particle radius in the calculations. This fact indicates that the oxygen exchange is influenced by the grain-boundary diffusion in addition to volume diffusion in this specimen. Fig. 4 illustrates an Arrhenius plot of D_a for

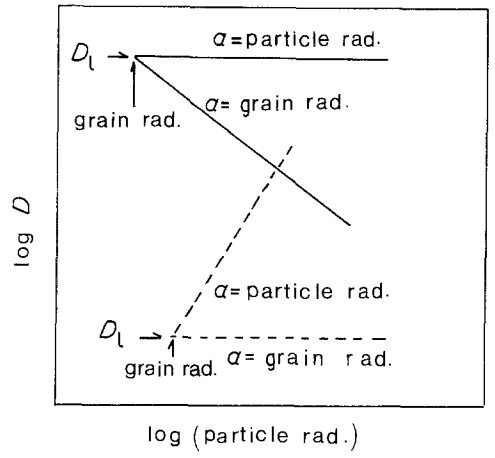

Figure 5 Schematic illustration of the relations between log D (D_a and D_l) against log (particle radius) for the two extreme cases of (---) $D_g \gg D_l$ and (——) $D_g = D_l$, where D_l is the volume diffusion coefficient and D_g is the grain-boundary diffusion coefficient.

specimen II with different particle sizes. In this case data points can be adjusted by a single straight line as long as the calculations were made using a = particle radius.

The relative magnitude of grain-boundary diffusion coefficient, D_g, with respect to volume diffusion coefficient, D_l, in polycrystalline particles may be divided into three categories [11], $D_g \gg D_l$, $D_g > D_l$ and $D_g = D_l$. In the case of $D_g \gg D_l$, D_g is so large that the concentration of ^{18}O along grain boundaries is nearly equal to that in an oxygen gas phase throughout a diffusion anneal [12, 13]. Equation 2 holds at a considered temperature in this case, independent of the particle sizes used, if the capacity of the boundaries is negligibly small with respect to that of the volume.

$$D_l/a_g^2 = C \quad (2)$$

where C is a constant. If the calculations of D_a are tentatively done in this case by taking a_p instead of a_g in Equation 2, one can obtain the following equation including a_p

$$D_a = a_p^2 C \quad \text{or} \quad \log D_a = 2 \log (a_p) + C' \quad (3)$$

In the case of $D_g = D_l$, on the other hand, Equation 4 holds for particles with different sizes [14]

$$D_l/a_p^2 = f(a_p) \quad (4)$$

In this case, if the calculations of D_a are tentatively made by taking a_g instead of a_p in Equation 4, D_a is expressed by

$$D_a = f(a_p)\, a_g^2 = D_l a_g^2/a_p^2 = C''/a_p^2$$

or

$$\log (D_a) = C''' - 2 \log (a_p) \quad (5)$$

In these two extreme cases linear relations always hold between log (D_a) and log (particle radius). This situation is schematically shown in Fig. 5.

Data of specimen I in Fig. 3 can be used to plot log (D_a) against log (particle radius). Fig. 6 shows the resultant linear plots; the upper plot is for the calculations of D_a as $a = a_p$, and the lower one, D_a as $a = a_g$. In comparing these plots with those in the two extreme cases (Fig. 5), we can say that diffusion in

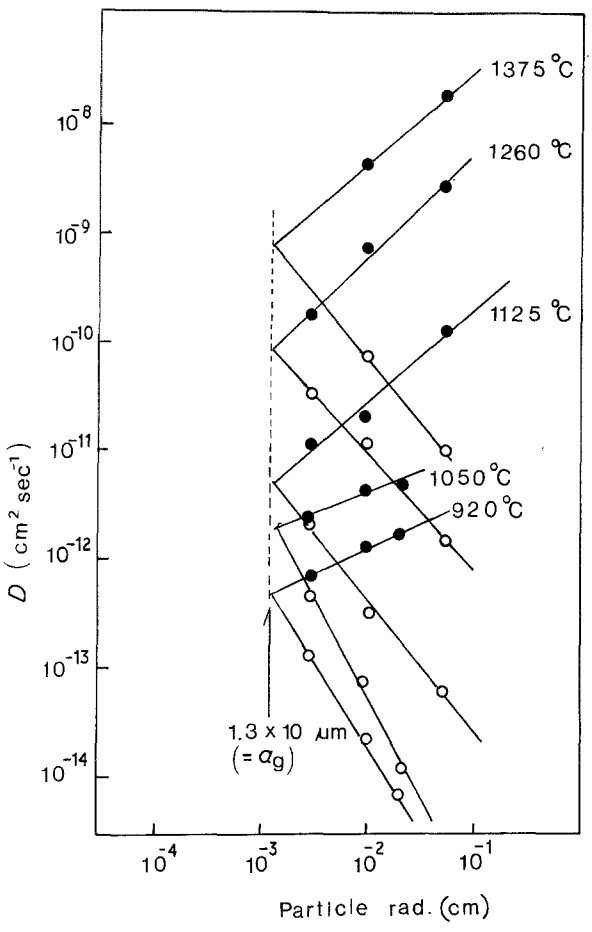

Figure 6 Plots of log (D_a) against log (a_p) for particles of specimen I at high temperatures. The calculations of D_a were made using (●) $a = a_p$ and (○) $a = a_g$ respectively.

specimen I falls between the two extremes, $D_g \gg D_l$ and $D_g = D_l$, now denoted as a category where $D_g > D_l$. If the respective two straight lines using a_g and a_p in Fig. 6 can be extrapolated down to the value of grain radius in the horizontal axis, D_a at this point should correspond to D_l [15]. It is emphasized that these two extrapolated lines do intersect to a grain radius that is identical to that of the experimentally measured grain radius (= 12.8). This fact indicates this way of calculating D_l using polycrystalline particles, to be plausible. The details of the reliability of this method were discussed in our previous paper [11]. One can thus make Arrhenius plots of oxygen volume diffusion coefficients for specimen I (Fig. 7). As seen there, two diffusion regions can be seen and they are respectively expressed by,

$$D_l = 2.4 \times 10^3 \exp\left[-\frac{429.0(\text{kJ mol}^{-1})}{RT}\right], \quad 1128°\text{C} \leqq T \leqq 1375°\text{C} \quad (6)$$

$$D_l = 2.4 \times 10^{-6} \exp\left[-\frac{153.2(\text{kJ mol}^{-1})}{RT}\right], \quad 920°\text{C} \leqq T < 1128°\text{C} \quad (7)$$

On the other hand, no particle-size dependence of D_a was observed in specimen II when the calculations of D_a were done by taking $a = a_p$. This fact indicates that $D_g = D_l$, and the resultant D_a can be regarded as D_l. The volume diffusion data are also shown in

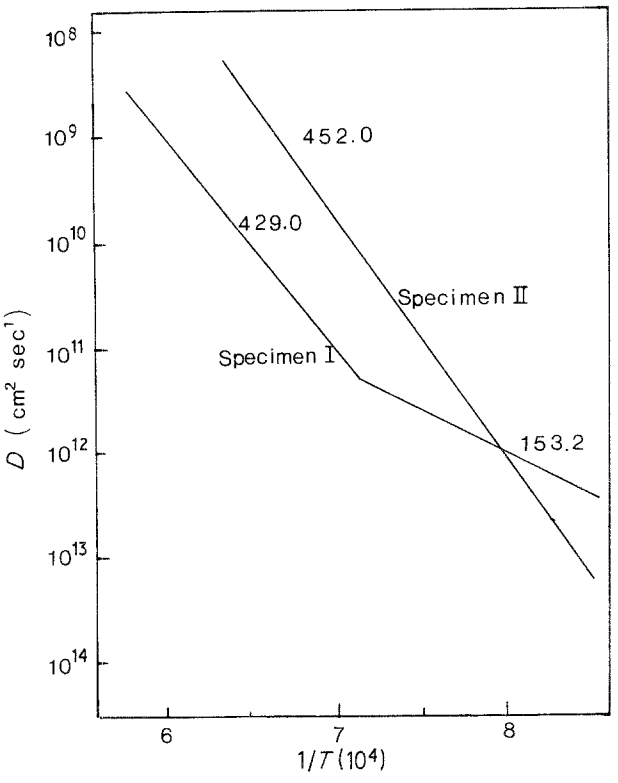

Figure 7 Arrhenius plots of volume diffusion coefficient of oxygen in particles of specimens I and II. Numbers on curves show activation energies in kJ mol^{-1}.

Fig. 7 together with the data of specimen I. They can be expressed by

$$D_I = 6.0 \times 10^6 \exp\left[-\frac{452.0(\text{kJ mol}^{-1})}{RT}\right], \quad 917°\text{C} \leqq T \leqq 1247°\text{C} \tag{8}$$

4. Discussion

4.1. Semiconducting behaviour at elevated temperatures

Many researchers in their electrical conductivity studies of rare-earth-doped perovskites such as barium titanate and strontium titanate under a high P_{O_2} range (≈ 1 atm $< P_{O_2} < \approx 10^{-8}$ atm) at elevated temperatures have considered an equation such as

$$La^{\cdot}_{(Ba)} + \tfrac{1}{2}Ba^{x}_{(Ba)} + Ti^{3+}_{(Ti^{4+})}{}' + \tfrac{1}{4}O_2 = \tfrac{1}{2}(BaO) + \tfrac{1}{2}V''_{Ba} + Ti^{4+}_{(Ti^{4+})}{}^{x} + La^{\cdot}_{(Ba)} \tag{9}$$

where the expression follows Verwey's notation. This indicates that the extra plus charge $La^{\cdot}_{(Ba)}$ is compensated by the preferential formation of Ti^{3+} (electronic compensation) with decreasing P_{O_2} and of V''_{Ba} (ionic compensation) with increasing P_{O_2}. Equation 9 results in

$$[n] \propto P_{O_2}^{-1/m} = P_{O_2}^{-1/4} \tag{10}$$

where $[n]$ is the concentration of electrons. Actually Balachandran and Error [16] in their electrical conductivity study of lanthanum-doped strontium titanate reported $m =$ to be 4.0 to 4.7, and Daniels and Hardtl [3] in their lanthanum-doped barium titanate study, $m = 3.7$, in a rough accordance with Equation 10. There is, however, no direct evidence as to the occurrence of defect structures in Equation 9.

Other probable equations in the high P_{O_2} region can also be considered as,

$$O_O = \tfrac{1}{2}O_2 + V^{\cdot}_O + e \tag{11}$$

$$O_O = \tfrac{1}{2}O_2 + V^{\cdot\cdot}_O + 2e \tag{12}$$

The mass action expression for Reaction 11 is

$$[V^{\cdot}_O][n] = K_1 P_O^{-1/2} = K'_1 P_O^{-1/2} \exp(-\Delta H_f/RT) \tag{13}$$

where ΔH_f is the standard enthalpy change of Reaction 11. One can obtain the following equation by giving two conditions, $[n] = [V^{\cdot}_O]$, and the mobility, μ, being constant with temperature

$$\sigma = e\mu[n] = K''_1 P_O^{-1/4} \exp(-\Delta H_f/2RT) \tag{14}$$

In a similar way, Reaction 12 results in

$$\sigma = K_2 P_O^{-1/6} \exp(-\Delta H'_f/3RT) \tag{15}$$

where $\Delta H'_f$ is the standard enthalpy change of Reaction 12.

The experimentally measured σ for specimen II was n-type with $-1/4.1$ dependence of P_{O_2} in the high P_{O_2} region cited (Fig. 1). This suggests a singly ionized oxygen vacancy also to be probable for the interpretation of the behaviour. However, the reported possibility of Equation 9 is not ruled out as far as only the numerical value of m is considered.

To examine the possibility of Reactions 11 or 12, oxygen volume diffusion data of the specimens may be useful. It was reported that oxygen diffusion in lanthanum-doped barium titanates progresses by an oxygen vacancy mechanism [9] as expected from a close-packed structure of the perovskites. Therefore, the oxygen volume diffusion coefficient can be taken as a measure of oxygen vacancy level. We have indicated in our oxygen diffusion study of lanthanum-doped barium titanates that a high-temperature oxygen diffusion with an activation energy of about 400 kJ mol^{-1} relates to thermal dissociation of the oxygen sublattice. The two activation energies, 429.0 kJ mol^{-1} for specimen I and 452.0 kJ mol^{-1} for specimen II in this study are believed to be the case. One can generally obtain a formation energy of oxygen vacancies by subtracting the corresponding migration energy from the present activation energy. The migration energy of specimen I ($x = 0.001$) can be taken as 153.2 kJ mol^{-1} (Equation 7). No extrinsic diffusion associated with the migration energy appeared for specimen II ($x = 0.01$). Fortunately the migration energy of a lanthanum-doped specimen with $x = 0.1$ had already been reported to be 65.3 kJ mol^{-1} [9]. It is likely that the migration energy for specimen II may fall between the foregoing two migration energies. Thus one can calculate values of $\Delta H_f/2$ in Equation 14 to be 149.4 to 193.3 kJ mol^{-1} for specimen II, because Reaction 11 should also be established in the temperature and P_{O_2} (= 50 mm Hg) conditions in diffusion annealings of the specimen.

In specimen I, on the other hand, the P_{O_2} dependence of σ in the runs at 1200 and 1250° C gave $\sigma \propto P_{O_2}^{-1/6.9}$. This numerical value suggests a doubly ionized oxygen vacancy mechanism for the cited conditions.

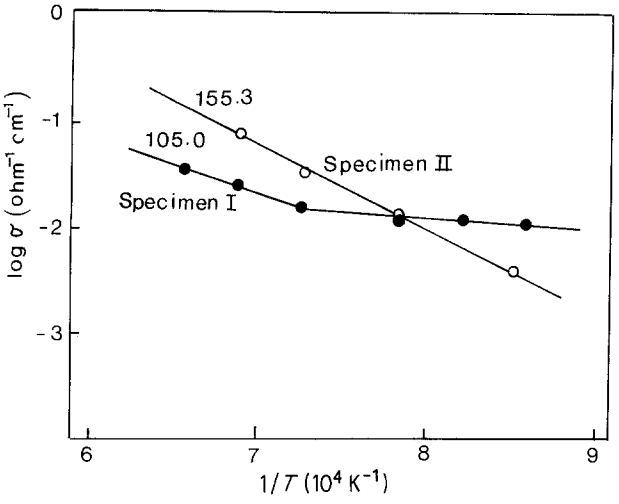

Figure 8 Arrhenius plots of electrical conductivity for specimens I and II. Numbers on curves show activation energies in kJ mol^{-1}.

Thus one can calculate $\Delta H_f'/3$ in Equation 15 using the two activation energies, 429.0 kJ mol^{-1} in the high-temperature diffusion and 153.2 kJ mol^{-1} in the low-temperature one to be 92.0 kJ mol^{-1} for specimen I.

On the other hand, one can also make Arrhenius plots of σ for the two specimens at P_{O_2} = 50 mm Hg at which diffusion data were also obtained, using data of Fig. 1 and some additional data, and the results are shown in Fig. 8. One can see two regions of σ in specimen I and a single region in specimen II. On comparing Figs 7 and 8, a qualitative relation of D_i between the two specimens is very similar to that of σ between the two. It should be noted that the two temperatures at which the respective two Arrhenius plots of diffusion and of σ intersect, are very close ($\approx$ 1000° C). These facts strongly suggest possible interpretation of σ in terms of oxygen vacancies over the whole temperature range studied. The two activation energies of σ at the high temperatures were 155.3 kJ mol^{-1} (specimen II) and 105.0 kJ mol^{-1} (specimen I), respectively. These two activation energies of σ for specimens I and II are close to those calculated from oxygen diffusion data using Equations 14 and 15. In summary, semiconducting behaviour at elevated temperatures of specimens I and II can successfully be interpreted in terms of ionized oxygen vacancy models in a P_{O_2} range 1 to 10^{-5} atm. This fact is in contrast with a controlled valency mechanism proposed for doped semiconducting perovskites.

Remarks may be necessary concerning the magnitude of σ for these two specimens and doped perovskites in general. Fig. 8 show that the level of σ at elevated temperatures above about 1000° C in specimen II is at most 3.3 times larger than that of specimen I, although the lanthanum-dopant level of the former is one order of magnitude larger than that of the latter. Such a disagreement has often been observed in many donor- [16, 17] and acceptor- [18] doped perovskites. Balachandran and Error [16], for an example, have reported in their study of lanthanum-doped strontium titanate that the measured σ value, in a plateau region appearing at a low P_{O_2} where σ becomes independent of P_{O_2}, is considerably lower than the value calculated assuming μ = 0.1 cm^2 sec^{-1} V^{-1} and $[n] = [\dot{La}_{(Sr)}]$ where μ is the mobility and $[n]$ is the concentration of electrons. Such a situation was also observed for a lightly lanthanum-doped barium titanate [7].

These facts also cast doubt on the controlled valency model of doped perovskites. Such a discrepancy is readily understandable if our model is considered. The value of σ is essentially associated with thermally formed ionized oxygen vacancies which form as a result of thermal dissociation of the oxygen sublattice. The degree of formation is dependent on the nature of oxygen–cation bonding of the perovskites. Our previous papers [8, 9] have shown that the existence of barium site vacancies in the doped material may play a decisive role in weakening the bond strength, even if other minor factors are also implicated. The lanthanum-doping in the form of over-stoichiometric composition "$Ba_{0.9}La_xTiO_{3+\delta'}$" ($x \geqq 0.1$) gave rise to a formula $(Ba_{x'}La_{y'}\square_{1-x'-y'})(Ti_{z'}\square_{1-z'})O_3$ in the calculations with two assumptions of states of +3 for lanthanum and +4 for titanium, where $\square$ denotes the cation vacancies, and the calculated and observed densities agreed well over the x values studied. One can therefore calculate defect structure formulae, $(Ba_{0.98836}La_{0.00998}\square_{0.0017})(Ti_{0.99834}\square_{0.00166})O_3$ for specimen II and $(Ba_{0.99884}La_{0.00099}\square_{0.00017})(Ti_{0.99983}\square_{0.00017})O_3$ for specimen I, respectively. The existence of barium-site vacancies with a large size may weaken the bond strength of the oxygen sublattice in the doped perovskites, which can accelerate the formation of ionized oxygen vacancies and electrons on firing the specimens. This idea was supported on the basis of oxygen diffusion data as a measure of oxygen vacancy level for the doped materials containing barium-site vacancies [8, 9]. According to such a model, there is no reason for $[n] = [\dot{La}_{(Ba)}]$ to hold even if $[n]$ is proportional to $[\dot{La}_{(Ba)}]$.

4.2. Electrical behaviour on cooling

Both specimens I and II exhibit semiconduction at elevated temperatures, as described. However, it is noticeable that the former remains semiconductive whereas the latter becomes insulative on cooling slowly to room temperature (Table I). The difference in σ at room temperature between the two is about eight orders of magnitude. It is necessary to clarify the origin of this behaviour to obtain a thorough understanding of the conducting behaviour of doped perovskites.

We can generally say that Reactions 11 and 12 go towards the left-hand side on cooling the doped materials, thus decreasing ionized oxygen vacancies. Care should be taken because preferential oxygen diffusion along grain boundaries occurred in specimen I whereas $D_g = D_i$ for specimen II, as described. Therefore such a preferential change from semiconduction to insulation on cooling specimen II cannot be explained in terms of preferential grain-boundary oxygen diffusion by which a decrease of oxygen vacancies and electrons progresses preferentially. Accordingly this phenomenon of interest should be understood by taking note of a structural change in the volume on the cooling.

One can see two regions of high and low tempera-

tures in the conductivity data of specimen I (Fig. 8). It is expected that such a high level of σ at the low temperature region for the specimen may be maintained down to considerably low temperatures, by which semiconduction can be exhibited even at room temperature. In specimen II, on the other hand, σ decreases appreciably with decreasing temperature (Fig. 8), enabling insulation to occur at room temperature.

It is emphasized again that a qualitative relation in the two diffusion curves in Fig. 7 is very similar to that in the two conductivity curves in Fig. 8. Therefore, the low-temperature conductivity in specimen I should also be explained in relation to oxygen vacancies. The maintenance of such a high σ down to room temperature in the specimen can be understood if ionized oxygen vacancies and electrons formed at elevated temperatures can exist metastably on cooling, by which their concentrations can hold roughly constant to room temperature. Generally the oxidation in Reactions 11 and 12 can progress to equilibrium in an oxygen atmosphere on cooling if both oxygen vacancies and electrons can move freely, by which their concentrations decrease. However, if movement of oxygen through oxygen vacancies is restricted, such a stabilization of oxygen vacancies and electrons can be expected. It is noted that the migration energy of oxygen increases with decreasing lanthanum dopant level, as was shown. The migration energies of specimen I with $x = 0.001$ and a specimen with $x = 0.1$ were 153.2 and 65.3 kJ mol^{-1}, respectively. The lower migration energy in the latter specimen compared with that in the former seems to be based on its open structure containing a higher level of cation vacancies in barium sites. Thus it seems that such a metastabilization seen in specimen I may be caused by difficulty in oxygen migration at lower temperatures. Further studies seem necessary for clarification of the origin of the metastabilization.

Let us again take note of Fig. 1 giving σ as a function of P_{O_2} for the two specimens. As seen there, log σ against log P_{O_2} plots for specimen II exhibit a normal behaviour as variation of σ, as well as the level of ionized oxygen vacancies, with both P_{O_2} and temperature occur equilibriumly down to a considerably low temperature. A peculiar feature of log σ against log P_{O_2} plots for specimen I can be seen at runs at lower temperatures. σ at 1000 and 1100° C is insensitive to P_{O_2}. Such a behaviour in lightly lanthanum-doped materials has also been reported by Chan and Smyth [17]. They interpreted the region insensitive to P_{O_2} at temperatures between 700 and 1000° C to be due to a pure controlled vacancy mechanism. It should be noted that no region insensitive to P_{O_2} was detected in runs at temperatures above 1200° C in this study. Therefore, interpretation of the P_{O_2}-insensitive region in terms of a controlled valency model may be ruled out. This peculiar behaviour insensitive to P_{O_2} is readily understandable if the above stabilization of oxygen vacancies and electrons occurs.

References

1. O. SABURI, *J. Phys. Soc. Jpn* **14** (1959) 1159.
2. G. G. HARMAN, *Phys. Rev.* **106** (1959) 1358.
3. J. DANIELS and K. H. HARDTL, *Philips Res. Rep.* **31** (1976) 489.
4. M. TSUKIOKA, personal communication (1986).
5. H. IKUSHIMA and S. HAYAKAWA, *Jpn J. Appl. Phys.* **6** (1967) 454.
6. K. KAKEGAWA, J. MOORI, I. TAKADA, K. TAKAHASHI and S. SHIRASAKI, *J. Chem. Soc. Jpn* **12** (1980) 1813.
7. S. SHIRASAKI, unpublished work.
8. S. SHIRASAKI, M. TSUKIOKA, H. YAMAMURA, H. OSHIMA and K. KAKEGAWA, *Solid State Commun.* **19** (1976) 721.
9. S. SHIRASAKI, H. YAMAMURA, H. HANEDA, K. KAKEGAWA and J. MOORI, *J. Chem. Phys.* **73** (1980) 4640.
10. J. CRANK, "The Mathematics of Diffusion" (Oxford University Press, London, 1957) p. 88.
11. S. SHIRASAKI, S. MATSUDA, H. YAMAMURA and H. HANEDA, *Adv. Ceram.* **10** (1985) 474.
12. K. KIJIMA and S. SHIRASAKI, *J. Chem. Phys.* **65** (1976) 2668.
13. H. HASHIMOTO, M. HAMA and S. SHIRASAKI, *J. Appl. Phys.* **43** (1971) 4828.
14. M. AKIYAMA, T. ANDO and Y. OISHI, *Rep. Design Prep. Functional Ceram.* **8** (1983) 11.
15. S. SHIRASAKI, I. SHINDO and H. HANEDA, *Chem. Phys. Lett.* **50** (1977) 459.
16. U. BALACHANDRAN and N. G. ERROR, *J. Electrochem.* **129** (1965) 1021.
17. N. H. CHAN and D. M. SMYTH, *J. Amer. Ceram. Soc.* **67** (1984) 285.
18. I. DANIELS, *Philips Res. Rep.* **31** (1976) 505.

Received 20 February
and accepted 29 April 1987